Establishing rod shape from spherical, peptidoglycan-deficient bacterial spores

Huan Zhang, Garrett Mulholland, Sofiene Seef, Shiwei Zhu, Jun Liu, Tam Mignot, Beiyan Nan

Establishing rod shape from spherical, peptidoglycan-deficient bacterial spores

Huan Zhang[a], Garrett A. Mulholland[a], Sofiene Seef[b], Shiwei Zhu[c,d], Jun Liu[c,d], Tâm Mignot[b], and Beiyan Nan[a,1]

[a]Department of Biology, Texas A&M University, College Station, TX 77843; [b]Laboratoire de Chimie Bactérienne, CNRS–Université Aix Marseille UMR7283, Institut de Microbiologie de la Méditerranée, 13009 Marseille, France; [c]Department of Microbial Pathogenesis, Yale University School of Medicine, New Haven, CT 06536; and [d]Microbial Sciences Institute, Yale University, West Haven, CT 06516

Edited by E. Peter Greenberg, University of Washington, Seattle, WA, and approved May 11, 2020 (received for review January 28, 2020)

Chemical-induced spores of the Gram-negative bacterium *Myxococcus xanthus* are peptidoglycan (PG)-deficient. It is unclear how these spherical spores germinate into rod-shaped, walled cells without preexisting PG templates. We found that germinating spores first synthesize PG randomly on spherical surfaces. MglB, a GTPase-activating protein, forms a cluster that responds to the status of PG growth and stabilizes at one future cell pole. Following MglB, the Ras family GTPase MglA localizes to the second pole. MglA directs molecular motors to transport the bacterial actin homolog MreB and the Rod PG synthesis complexes away from poles. The Rod system establishes rod shape de novo by elongating PG at nonpolar regions. Thus, similar to eukaryotic cells, the interactions between GTPase, cytoskeletons, and molecular motors initiate spontaneous polarization in bacteria.

germination | Rod system | MreB | GTPase | gliding motor

Morphogenesis is a fundamental feature of cells. Compared to spheres that are symmetric in all directions, rods are asymmetric and polarized. For most rod-shaped bacteria, the peptidoglycan (PG) cell wall defines cell geometry, which is assembled by two major enzymatic systems. The Rod system consists of RodA, a SEDS-family PG polymerase, PBP2, a member of the class B penicillin-binding proteins (bPBPs), and MreB, a bacterial actin homolog that orchestrates the activities of the Rod complexes in response to local cell curvature (1). In contrast, class A PBPs (aPBPs) contribute to PG growth independent of MreB (2, 3).

Myxococcus xanthus, a rod-shaped Gram-negative bacterium, utilizes polarized geometry for directed locomotion. MglA, a Ras family small GTPase, controls the direction of gliding motility (4–7). As cells move, GTP-bound MglA forms large clusters at leading cell poles, whereas GDP-bound MglA distributes homogeneously in the cytoplasm (4, 6, 7). MglA-GTP stimulates the assembly of the gliding machineries through direct interaction with MreB (7–10) and directs the gliding machineries toward lagging cell poles (5). Consequently, the gliding machineries carry MreB filaments as they move rapidly in the membrane (11–13). The activity of MglA is regulated by its cognate GTPase-activating protein (GAP), MglB, which forms large clusters at lagging cell poles. MglB activates the GTPase activity of MglA, expelling MglA-GTP and, thus, the assembled gliding machineries, from lagging poles (4, 6). Overall, polarized localization and activities of MglA and MglB ensure that the gliding machineries generate propulsion by moving from poles to nonpolar regions (5, 7, 14).

Some rod-shaped bacteria change their geometry through sporulation. In Firmicutes such as Bacilli and Clostridia, the morphological differentiation from rod-shaped vegetative cells to oval spores begins with an asymmetric division, resulting in the formation of a smaller endospore wholly contained within a larger mother cell. In contrast to endospore-forming bacteria, *M. xanthus* produces spores using two division-independent mechanisms. First, groups of vegetative cells can aggregate on solid surfaces and build spore-filled fruiting bodies in a few days (15). Second, individual *M. xanthus* cells can form dispersed, spherical spores within hours in response to chemical signals, such as glycerol (16). Unlike endospores that contain intact and often thickened PG (17, 18), glycerol-induced *M. xanthus* spores are PG-deficient. Using high-performance liquid chromatography (HPLC) and transmission electron microscopy (TEM), Bui et al. found that such spores contained no detectable muropeptides (19). Consistent with the absence of PG, agents that inhibit PG synthesis or disrupt PG, including β-lactams, D-cycloserine, fosfomycin, and hen egg-white lysozyme, induce spore formation at low concentrations and the formed spores are naturally resistant to these agents (20). Without the polarity defined by PG, the mechanism by which these spores elongate into rods remains largely unknown.

Results

Two-Phase Morphological Transition during *M. xanthus* Spore Germination. Overnight induction of WT cells by 1 M glycerol produced sonication-resistant spores with length-to-width aspect ratios (L/W) of 1.6 ± 0.4 (n = 789), among which 40.9% are approximately spherical (L/W ≤ 1.3). Overall, the L/W values of most (85.4%) spores were lower than 2. As spores germinated, the morphological transition progressed in a two-phase manner. In the first hour (Phase I), L/W did not change significantly ($P = 0.57$, Fig. 1 *A* and *B*, Movie S1, and *SI Appendix*, Table S1). After 1 h, L/W increased sharply as emerging cells transformed

Significance

Spheres and rods are among the most common shapes adopted by walled bacteria, in which the peptidoglycan (PG) cell wall largely determines cell shape. When induced by chemicals, rod-shaped vegetative cells of the Gram-negative bacterium *Myxococcus xanthus* thoroughly degrade their PG and shrink into spherical spores. As these spores germinate, rod-shaped cells are rebuilt without preexisting templates, which provide a rare opportunity to visualize de novo PG synthesis and polarization. In this study, we investigated how spherical spores germinate into rods and elucidated a system for rod-shape morphogenesis that includes the Rod PG synthesis system, a GTPase-GAP pair, the MreB cytoskeleton, and a molecular motor. Such mechanisms for cell polarization might have evolved before the divergence between prokaryotes and eukaryotes.

Author contributions: H.Z. and B.N. designed research; H.Z., G.A.M., S.Z., and B.N. performed research; S.S. and T.M. contributed new reagents/analytic tools; H.Z., S.Z., J.L., and B.N. analyzed data; and H.Z., S.Z., T.M., and B.N. wrote the paper.

The authors declare no competing interest.

This article is a PNAS Direct Submission.

Data deposition: The codes used for cell dimension measurement and dynamic analysis of protein clusters are deposited in the GitHub repository, https://github.com/NanLabMyxo/Rod_shape_paper.

[1]To whom correspondence may be addressed. Email: bnan@tamu.edu.

This article contains supporting information online at https://www.pnas.org/lookup/suppl/doi:10.1073/pnas.2001384117/-/DCSupplemental.

First published June 8, 2020.

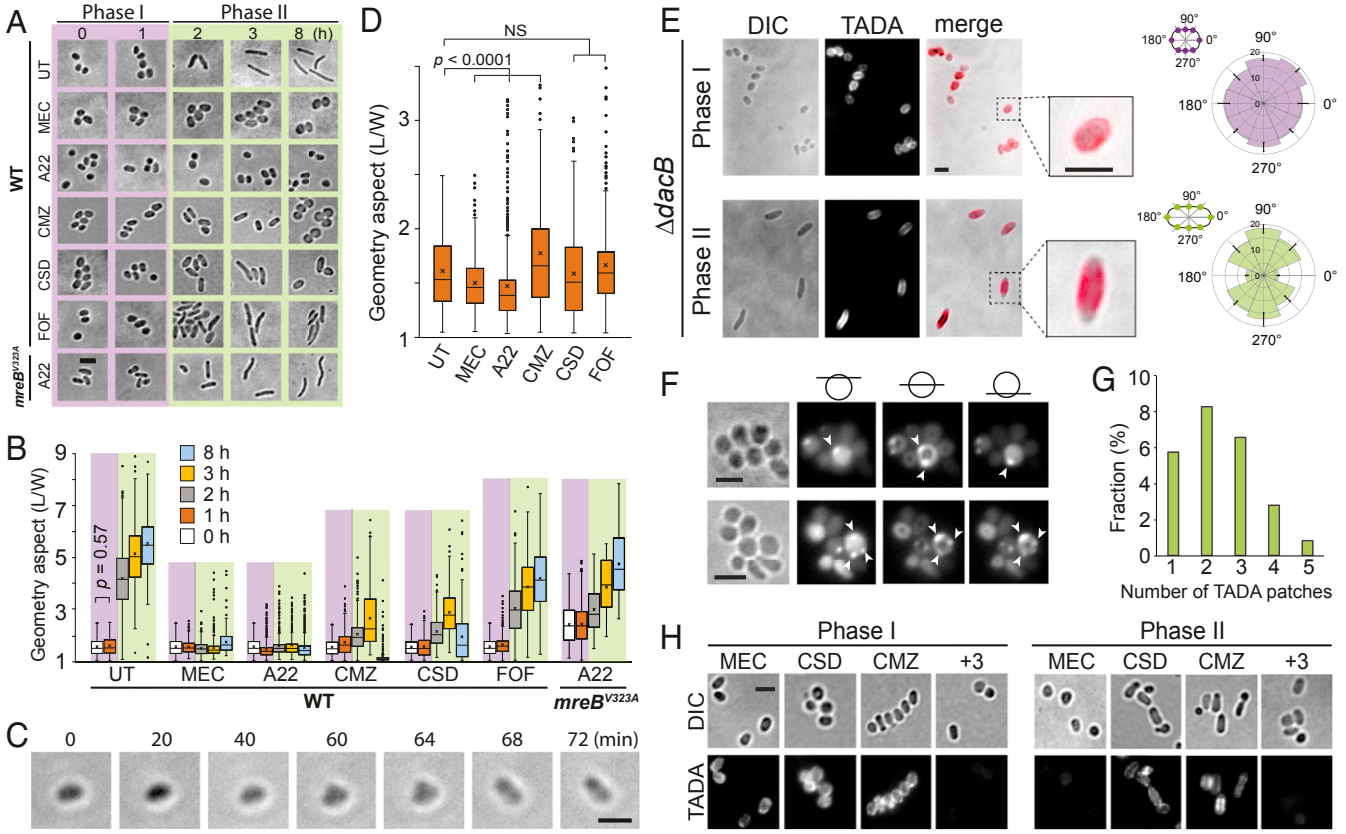

Fig. 1. PG polymerization by the Rod system is essential for de novo establishment of rod shape. (*A*) Morphological changes of untreated (UT) and inhibitor-treated spores in the germination process. A22 (100 μg/mL), mecillinam (MEC, 100 μg/mL), cefmetazole (CMZ, 5 mg/mL), cefsulodin (CSD, 5 mg/mL), and fosfomycin (FOF, 8 mg/mL). (*B*) Quantitative analysis of the germination progress using the aspect ratios (L/W) of spores/cells. Boxes indicate the 25th–75th percentiles, whiskers the 5th–95th percentiles. In each box, the midline indicates the median and × indicates the mean (same below, *SI Appendix*, Table S1). Outlier data points are shown as individual dots above and below the whiskers. (*C*) An oval spore initiates elongation along its short axes (Movie S2). (*D*) Phase I spores become more spherical after 1-h treatments by A22 and mecillinam. Cefmetazole-treated spores initiate elongation earlier than untreated ones. (*E*) Patterns of PG growth in both phases of germination were visualized by TADA in Δ*dacB* spores. The average and SD of TADA intensity were calculated from 20 spores/cells in the diagrams to the right (same below). (*F*) Imaged at different focal planes, 22.0% of Phase I spores show bright TADA patches (arrowheads) that position randomly on spore surfaces. (*G*) Among these 22.0% spores, many contain multiple TADA patches. (*H*) Compared to untreated (UT) Δ*dacB* spores, while neither MEC, CMZ, or CSD is able to block PG growth, the combination of all three antibiotics (+3) abolishes PG growth in Phase I of germination. In contrast, MEC alone is sufficient to inhibit PG growth in Phase II. (Scale bars, 2 μm.) *P* values were calculated using the Student paired *t* test with a two-tailed distribution (same below). NS, nonsignificant difference.

into rods (Phase II). Importantly, 40.2% ($n = 244$) of spores did not initiate elongation along their original long axes (Fig. 1*C* and Movie S2), indicating that although not perfectly spherical, the geometry of mature spores does not predetermine the polarity of emerging cells. After 3 h, 70.2% ($n = 198$) of emerging cells reached the dimensions of vegetative cells. After 8 h, the whole population of emerging cells is indistinguishable from vegetative cells (L/W = 5.6 ± 1.1, $n = 233$; Fig. 1 *A* and *B*, Movie S1, and *SI Appendix*, Table S1). Consistent with the report by Bui et al. that mature glycerol-induced spores do not contain detectable muropeptides (19), the spores obtained under our sporulation conditions do not retain intact PG layers (*SI Appendix*, Fig. S1). Among 15 spores imaged using cryo-electron tomography (cryo-ET), only one shows discontinuous densities that could represent PG fragments (*SI Appendix*, Fig. S1*C*).

The Rod System Plays Major Roles in the De Novo Establishment of Rod Shape. The Rod complexes are the major machineries for PG elongation in *Escherichia coli* and *Bacillus subtilis* (1). To investigate the role of PG growth, especially the function of the Rod system in the de novo establishment of rod shape, we fused a DNA sequence encoding mCherry to the endogenous *rodA* gene in the WT background. The resulted strain showed minor delay of elongation during sporulation and was able to establish rod shape, indicating that the mCherry-labeled RodA retains its enzymatic activity (*SI Appendix*, Fig. S2 and Table S1). RodA-mCherry formed clusters in vegetative cells (*SI Appendix*, Fig. S2), which when imaged at 3.33 Hz, showed typical diffusion, with diffusion coefficients (D_{RodA}) of (3.1 ± 2.0) × 10^{-2} μm^2/s ($n = 160$) (Movie S3). Mecillinam is a β-lactam that specifically inhibits PBP2 in the Rod system. Similar to *E. coli*, mecillinam-treated *M. xanthus* cells produced bulges on their surfaces and eventually lysed (Fig. 1 *A* and *B* and *SI Appendix*, Fig. S3*A* and Table S1). Consistent with a previous report in *E. coli* that the diffusion of PBP2 does not correlate with its catalytic activity (21), mecillinam treatment did not affect the diffusivity of RodA clusters in *M. xanthus* (D = (3.4 ± 2.1) × 10^{-2} μm^2/s, $n = 58$, $P = 0.39$) (Movie S4). Despite its negligible effect on diffusion, mecillinam significantly inhibited the formation of RodA clusters. During 150-s of imaging at 0.33 Hz, untreated vegetative cells in the exponential phase formed 10.1 ± 3.4 RodA clusters per cell ($n = 50$). In the presence of mecillinam, this number decreased to 3.1 ± 1.1 clusters per cell ($n = 71$) (*SI Appendix*, Fig. S3 *B* and *C*). Based on the above observations, we reasoned that

the formation of RodA clusters, rather than their diffusion, correlates with the activity of Rod complexes. Consistent with disrupted function of the Rod system, *M. xanthus* spores were not able to elongate into rods in the presence of mecillinam (Fig. 1 *A* and *B* and *SI Appendix*, Table S1).

A22, an inhibitor of MreB that causes the loss of rod shape and cell lysis (9, 11), also inhibits the formation of RodA cluster in WT cells but not in the cells where the original MreB was replaced by MreB^{V323A}, an A22-resistant variant (9) (*SI Appendix*, Fig. S3). The similarity between the inhibitory effects of A22 and mecillinam suggests that like in other bacteria, MreB is an essential component in the Rod system of *M. xanthus*. Treated by A22, WT spores failed to germinate into rods as their L/W ratios did not increase within 8 h. In contrast, A22-resistent spores were able to elongate into rods in the presence of A22, indicating that A22 inhibits germination specifically through MreB (Fig. 1 *A* and *B* and *SI Appendix*, Table S1). Both A22 and mecillinam-treated spores were viable because they were able to grow into rods when transferred into inhibitor-free medium. Since these spores became even more spherical in Phase I (Fig. 1*D*), neither A22 nor mecillinam blocked the hydrolysis of spore coats that maintain the shape of oval spores. Vegetative *M. xanthus* cells are sensitive to fosfomycin, an antibiotic that inhibits the production of UDP-MurNAc, a precursor of PG (11). As spores preserve PG precursors (19), they were able to elongate into rods in the presence of fosfomycin, albeit at reduced rates (Fig. 1 *A* and *B* and *SI Appendix*, Table S1). Taken together, PG polymerization by the Rod system is essential for the establishment of rod-shape.

Two-Phase PG Growth during *M. xanthus* Spore Germination. As the pathways for PG synthesis are largely conserved, fluorescent D-amino acids (FDAAs) have been used as proxy reporters for

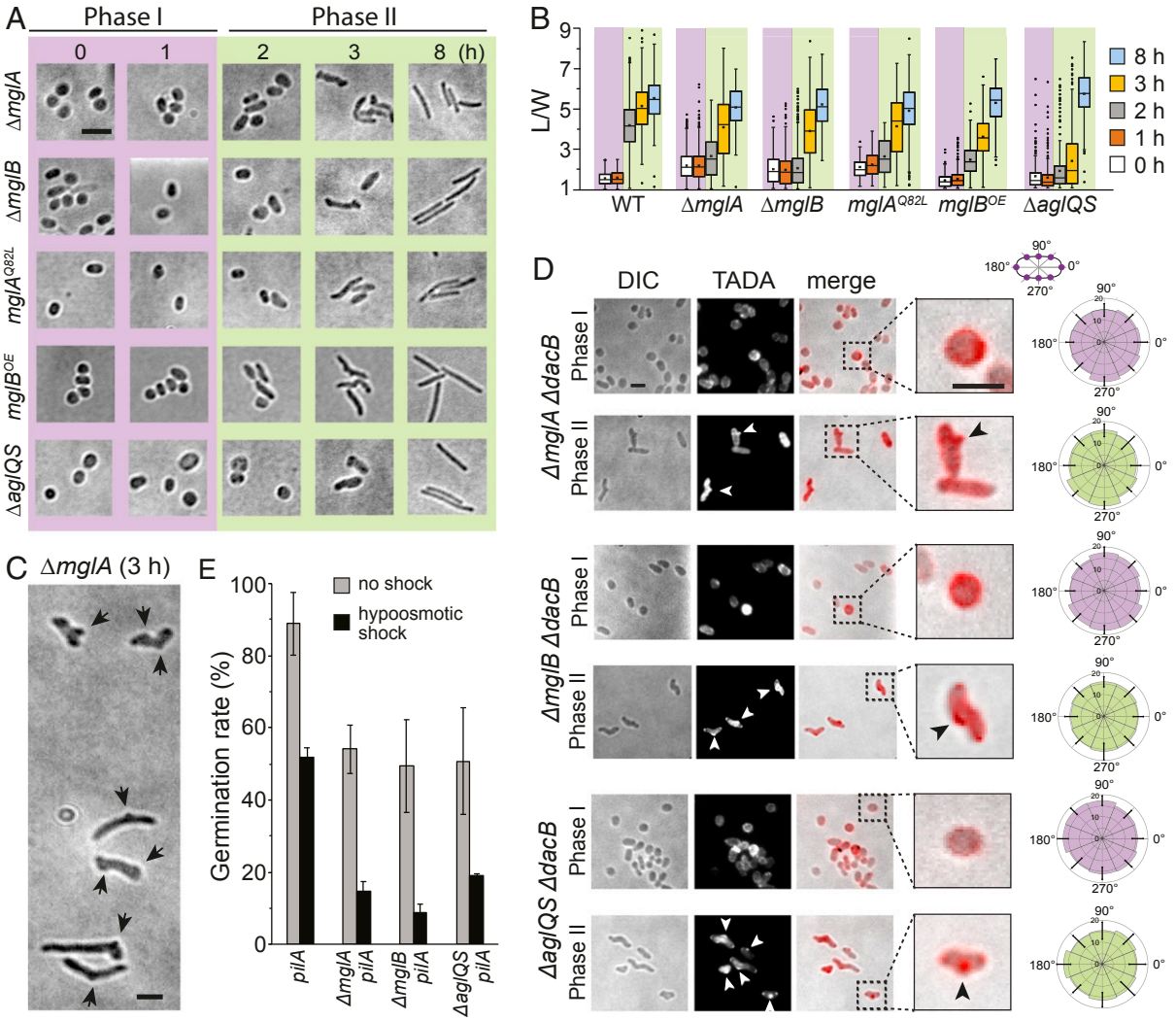

Fig. 2. MglA and MglB are required for rapid cell elongation. (*A*) Emerging cells from Δ*mglA*, Δ*mglB*, *mglA*^{Q82L}, and *mglB*^{OE} spores and Δ*aglQS* pseudospores show significant delay in elongation and bulges on cell surfaces in Phase II of germination. (*B*) Quantitative analysis of the germination progress. (*C*) A representative image of the altered morphology of the emerging Δ*mglA* cells after 3 h of germination. Arrows point to the bulges on cell surfaces. (*D*) The disruption of either the MglA-MglB polar axis (Δ*mglA* Δ*dacB* and Δ*mglB* Δ*dacB*) or the gliding motor (Δ*aglQS* Δ*dacB*) resulted in significantly higher TADA staining at cell poles and budges (arrowheads) in Phase II. To visualize PG growth in Phase I, we added TADA to the medium at the beginning of germination and allowed Δ*dacB* spores to germinate for 1 h. To visualize PG growth in Phase II, we allowed spores to germinate for 1 h before adding TADA into the medium, then imaged the pattern of PG growth after 1 h of incubation in the presence of TADA. Quantitative analysis of TADA fluorescence from 20 cells in each germination phase is shown at *Right*. (*E*) The disruption of either the MglA-MglB polar axis (Δ*mglA pilA::tet* and Δ*mglB pilA::tet*) or the gliding motor (Δ*aglQS pilA::tet*) significantly decreases the survival rate of germinating spores (gray bars), especially under osmotic stress (black bars). Spores were subject to hypoosmotic shock (20 mM Tris·HCl, pH 7.6) for 1 h after 1 h of germination. (Scale bars, 2 μm.)

PG growth in many bacteria (22, 23). *B. subtilis* (Gram-positive) and *E. coil* (Gram-negative) incorporate single D-amino acid–based fluorescent probes into PG using transpeptidases that catalyze the last steps of PG polymerization (24). We postulate that *M. xanthus* incorporates FDAAs in a similar manner. First, the PG synthesis pathway of *M. xanthus* is similar to that of *B. subtilis* and *E. coli* (25). Second, the incorporation of a fluorescent D-amino acid, TAMRA 3-amino-D-alanine (TADA) (26), is blocked by β-lactams that inhibit transpeptidases (see below). We visualized the patterns of PG growth using TADA to label the positions of PG enzymatic activity. To enhance labeling efficiency, we deleted the *dacB* gene (*mxan_3130*), which encodes a D-Ala-D-Ala carboxypeptidase (22). The resulted Δ*dacB* cells showed identical morphology to the WT ones and produced sonication-resistant spores. The Δ*dacB* spores showed minor delay in germination and efficient TADA incorporation (Fig. 1*E* and *SI Appendix*, Fig. S2 and Table S1).

Although L/W of spores did not change in Phase I, PG had started to grow. After 1 h of germination in the presence of TADA, the surfaces of most Phase I-emerging cells (78.0%, n = 600) were evenly labeled by fluorescence (Fig. 1*E*). The remaining 22.0% of Phase I cells showed patches of TADA (Fig. 1*F*). However, these patches do not likely register future poles because 47.0% (n = 132) of such spores contained more than two TADA patches, and these patches positioned randomly on spore surfaces (Fig. 1 *F* and *G*). In contrast, as cells grew into rods, TADA was incorporated heavily at nonpolar regions and fluorescence signals were generally absent at cell poles (Fig. 1*E*). The patterns of PG growth indicate that spores first synthesize PG on their spherical surfaces in Phase I and then break symmetry in Phase II by growing PG at nonpolar regions.

In Phase I of germination, TADA was incorporated into PG in the presence of mecillinam (Fig. 1*H*). Neither cefsulodin nor cefmetazole, the β-lactams that inhibit PBPs other than PBP2 in *E. coli* (3), blocked TADA incorporation in Phase I *M. xanthus* cells. However, a combination of mecillinam, cefsulodin, and cefmetazole abolished TADA incorporation (Fig. 1*H*). These results suggest that cefsulodin and cefmetazole might inhibit aPBPs in *M. xanthus* and that both aPBPs and the Rod system contribute to the isotropic PG growth in Phase I. Consistent with this result, spores were able to form rods in the presence of cefsulodin and cefmetazole, albeit the elongation rate was slower (Fig. 1 *A* and *B* and *SI Appendix*, Table S1). In contrast, mecillinam alone was sufficient to block TADA incorporation in Phase II of germination (Fig. 1*H*). In agreement with a recent report that cells reduce their diameter when the Rod system becomes dominant over other PBPs (27), emerging cells continued to grow in length but shrink in width in Phase II (*SI Appendix*, Fig. S3 and Table S1). These results confirm that while both non-Rod PBPs and the Rod system participate in PG synthesis during germination, the Rod system plays major roles in cell elongation.

Despite successful elongation in early Phase II (1–3 h), 57.2% (n = 215) of cefsulodin-treated and 96.6% (n = 203) cefmetazole-treated emerging cells retrogressed to spheres after 8-h treatments (Fig. 1 *A* and *B* and *SI Appendix*, Table S1), which is in agreement with a recent report that non-Rod PBPs, especially aPBPs, are required for the mechanical stability of cells (28). L/W values of the cefmetazole-treated spores increased significantly in Phase I of germination ($P < 0.0001$, Fig. 1 *B* and *D* and *SI Appendix*, Table S1), suggesting that cells elongate earlier when PBP2 is dominant over other PBPs. The inhibitory effects of cefsulodin and cefmetazole and the coordination between PG synthesis systems still remain to be fully understood. On the one hand, since cefsulodin and cefmetazole reduce the elongation rates of emerging cells (Fig. 1 *A* and *B* and *SI Appendix*, Table S1), the targets of these antibiotics, potentially non-Rod PBPs, still participate in PG synthesis in Phase II of germination. However, the activities of these PBPs might depend on the Rod system because mecillinam alone is sufficient to block TADA incorporation in Phase II.

MglA and MglB Are Required for Rapid Cell Elongation. To investigate how *M. xanthus* spores establish rod shape de novo, we tested the potential roles of polar-localized motility regulators. Δ*mglA* and Δ*mglB* cells were able to form sonication-resistant spores, but their spores showed severe delays in elongation, especially in early Phase II of germination. After 3 h, only 15.7% of the Δ*mglA* (n = 140) and 10.4% of Δ*mglB* (n = 298) cells reached the vegetative aspect ratio (comparing to 70.2% of WT cells, Fig. 2 *A* and *B* and *SI Appendix*, Table S1). In contrast, deleting *romR* and *plpA*, the genes encode two additional polar-localized motility regulators (29–31), only caused minor delay in germination (*SI Appendix*, Fig. S2 and Table S1). Both the Δ*mglA* and Δ*mglB* spores were able to elongate in length and shrink in width, albeit at significantly lower rates (Fig. 2 *A* and *B* and *SI Appendix*, Table S1 and Fig. S4), indicating that PG growth by the Rod complex still occurred. Strikingly different from WT spores that maintained relatively smooth cell surfaces during germination, cells from the Δ*mglA* and Δ*mglB* spores showed pronounced bulges at nonpolar regions in early Phase II, appearing to have multiple cell poles (Fig. 2 *A* and *C* and Movie S5). However, this morphological defect disappeared after prolonged growth (8 h) (Fig. 2*A*), implying that a system independent of MglA and MglB was able to correct morphological defects, although much less robustly. To determine how MglA and MglB regulate germination, we investigated the spores that expressed the $MglA^{Q82L}$ variant as the sole source of MglA, under the control of the native promoter of the *mglBA* operon. $MglA^{Q82L}$ expresses normally but is unable to hydrolyze GTP, resembling a loss-of-function allele (6). Spores expressing WT MglB and $MglA^{Q82L}$ were sonication-resistant but showed both a severe delay in cell elongation and bulged surfaces on emerging cells, similar to the Δ*mglA* and Δ*mglB* spores (Fig. 2 *A* and *B* and *SI Appendix*, Table S1). Surprisingly, overproducing MglB ($mglB^{OE}$), which potentially overstimulates the GTPase activity of MglA, caused similar defects during germination (Fig. 2 *A* and *B* and *SI Appendix*, Table S1). Thus, fine-tuned GTPase activity of MglA is required for rapid cell elongation and MglB functions through MglA.

Both the delayed morphological transition and bulged surfaces of the emerging Δ*mglA* and Δ*mglB* cells suggest that MglA and MglB might regulate PG growth during germination. Δ*mglA* Δ*dacB* and Δ*mglB* Δ*dacB* spores were able to grow PG in an isotropic manner in Phase I, indistinguishable from the Δ*dacB* spores (Fig. 2*D*). However, emerging cells from both mutant spores displayed elevated PG growth at cell poles and bulges in Phase II (Fig. 2*D*).

To test if delayed elongation and uneven PG growth during germination reduce the viability of Δ*mglA* and Δ*mglB* spores, especially under osmotic stresses, we enumerated spores in cell-counting chambers and calculated their viability by dilution plating. To simplify cell counting, *pilA* was disrupted by plasmid insertion (*pilA::tet*) to reduce cell aggregation (32). As shown in Fig. 2*E*, compared to the *pilA::tet* spores that 89 ± 9% (calculated from three independent experiments, same below) formed colonies, both Δ*mglA pilA::tet and* Δ*mglB pilA::tet* spores formed colonies at reduced rates (54 ± 7% and 49 ± 13%, respectively). To further test if altered growth pattern reduces the strength of PG, we allowed spores to germinate for 1 h, then incubated emerging cells in a hypoosmotic buffer (20 mM Tris·HCl, pH 7.6) for 1 h before plating. Hypoosmotic shock reduced the survival rate of *pilA::tet* emerging cells to 52 ± 3%, indicating that the still-growing PG in germination Phase II is sensitive to osmotic stress. Strikingly, after hypoosmotic shock, less than 15% of Δ*mglA pilA::tet* (15 ± 3%) and Δ*mglB pilA::tet* (9 ± 2%) emerging cells formed colonies (Fig. 2*E*). Consistent with the

minor roles of PlpA and RomR in germination, 50 ± 8% of Δ*plpA pilA::tet* and 41 ± 5% of Δ*romR pilA::tet* emerging cells formed colonies after hypoosmotic shock, similar to the survival rate of *pilA::tet* cells. Taken together, the MglA-MglB polarity axis regulates PG growth in Phase II of germination, which plays important roles in the survival of glycerol-induced *M. xanthus* spores.

MglB Stabilizes at the First Future Pole. We expressed YFP-labeled MglA as merodiploids in the WT background (6, 9) and mCherry-labeled MglB (stably expressed, *SI Appendix*, Table S1 and Fig. S2) in the Δ*mglB* mutant and investigated their localization patterns in regard to germination progress (L/W). Spores from neither strain showed significant defects in germination (*SI Appendix*, Table S1 and Fig. S2). Most (94.1%, $n = 152$) of Phase I spores (L/W ≤ 2) contained one or two MglB clusters (Fig. 3 *A* and *B*). In Phase II spores (L/W > 2), this ratio increased to 100% ($n = 120$). In contrast, MglA did not form clusters until Phase II, when 54.2% of emerging cells contained one or two MglA clusters (Fig. 3 *A* and *B*). Thus, during germination, MglB establishes polarized localization prior to MglA.

To test if the clusters of MglB in Phase I spores mark the polarity inherited from previous vegetative cells, we imaged MglB clusters at 0.05 Hz. Surprisingly, the majority of MglB clusters in Phase I spores was highly dynamic (Fig. 3*C* and Movie S6). Among 114 MglB clusters in Phase I spores, 22.9% remained stationary, and 77.1% showed typical diffusion, with diffusion coefficients (D_{MglB}) of $1.1 \times 10^{-4} \pm 4.6 \times 10^{-5}$ μm^2/s. These "wandering" MglB clusters were observed in both the approximately spherical (L/W < 1.3) and oval spores (1.3 < L/W ≤ 2), which supports our hypothesis that, regardless of their geometry, polarity is not yet established in Phase I spores.

As germination progressed, MglB clusters started to stabilize. Strikingly, once stabilized, the locations of MglB clusters became one of the cell poles for cell elongation (Fig. 3*D* and Movie S7). In Phase II of germination (L/W > 2), the population of stationary MglB clusters increased from 22.9 to 76.4% ($n = 106$, Fig. 3*E*). Stabilized MglB clusters began to oscillate between newly established poles (Fig. 3*C* and Movie S8), which might ensure that MglB occupies each future cell pole for an equal amount of time. As MglB clusters stabilized, MglA started to form clusters. The formation of MglA-YFP clusters was delayed significantly in the Δ*mglB* background, and only 23.3% ($n = 120$) of emerging cells contained MglA clusters in Phase II of germination (Fig. 3 *A* and *B*). Among the 204 cells in which both proteins formed single clusters, 176 (86.3%) positioned MglA and MglB clusters at opposite poles (a representative group of cells is shown in Fig. 3*F*). Thus, spherical spores start to elongate into rods along the axes established by the sequential stabilization of MglB and MglA clusters.

To investigate whether the stabilization of MglB clusters is predetermined by local cell curvatures, we quantified the localization of stationary MglB clusters with regard to the geometry of spores. We divide each spore/cell envelope into four quarters. In the quarter that contained stationary MglB clusters, we defined the long and short axes as 0° and 90°, which mark the local curvature that shows the highest and lowest similarity to the poles of vegetative cells, respectively. As shown in Fig. 3*G*, MglB clusters stabilized randomly in Phase I spores, indicating that local curvature does not dictate the localization of MglB. After the stabilization of MglB, the sites harboring MglB clusters transformed into cell poles (0°) in Phase II (Fig. 3*G*).

MglB clusters could stabilize at the sites where PG synthesis has completed or not yet initiated. We ruled out the second possibility because the majority of MglB clusters (76.4%, $n = 106$) stabilizes at poles in Phase II (Fig. 3 *A* and *B*), where almost no TADA incorporation was observed later (Fig. 1*E*). In both phases of germination, the population of static MglB clusters increased dramatically in the presence of A22 and mecillinam (Fig. 3*E*). Taken together, it is the Rod system, rather than the geometry of the spore, that regulates the dynamic of MglB clusters. As MglB clusters only stabilize at the sites where the Rod system is inactive, a region where PG synthesis by the Rod system completes first in Phase I will become a future cell pole in Phase II.

The MglA-MglB Polarity Axis Regulates the Distribution of the Rod System. As the Rod complex is the major system for PG growth in Phase II, the MglA-MglB polarity axis might regulate cell elongation through the Rod complexes. However, MglA and MglB are both cytoplasmic proteins, which are not likely to regulate the periplasmic activities of the Rod system directly. To investigate whether MglA and MglB regulate the distribution of the Rod complexes in Phase II of germination, we expressed RodA-mCherry endogenously in Δ*mglA* and Δ*mglB* spores. Along the long axis of the emerging cells, we loosely defined a region within 320 nm from each end of cell as a "pole" (which contains the cell pole and its adjacent subpolar region) and the rest of the cell as the "nonpolar region." In the emerging cells from WT spores that expressed RodA-mCherry, the ratio between nonpolar and polar-localized RodA clusters was 1.45 ($n = 387$, Fig. 4*B*). In contrast, in the Δ*mglA* and Δ*mglB* backgrounds, this ratio decreased to 0.52 ($n = 442$) and 0.53 ($n = 787$), respectively (Fig. 4*B*). Our data support the hypothesis that during the sphere-to-rod transition, the established MglA-MglB axis expels the Rod system from cell poles.

The MglA-MglB Polarity Axis Regulates the Distribution of Rod Complexes through MreB and the Gliding Motor. The diffusion of RodA and MglB clusters is not likely connected. First, D_{RodA} is two orders of magnitude higher than D_{MglB}. Second, the majority of MglB clusters only diffuses in Phase I of germination while RodA clusters diffuse during both germination and vegetative growth. Thus, the MglA-MglB polarity axis does not likely regulate the distribution of Rod complexes directly. Since MglA binds to MreB in the Rod complex, and the disruption of the MreB filaments inhibits the formation of RodA clusters (*SI Appendix*, Fig. S3), we hypothesized that the MglA-MglB polarity axis could regulate the distribution of Rod complexes through MreB. Although a photoactivatable mCherry (PAmCherry)-labeled MreB variant fully supports WT growth rate in vegetative cells (11), when expressed as the sole source of MreB, it failed to support rapid cell elongation in Phase II of germination. Nevertheless, spores expressing MreB-PAmCherry as merodiploids showed WT germination kinetics (*SI Appendix*, Fig. S2 and Table S1), which were used to visualize the localization of MreB. When exposed to 405-nm excitation (0.2 kW/cm^2) for 2 s, the majority of PAmCherry was photoactivated (11, 13). MreB-PAmCherry localized diffusively in Phase I spores, and we were not able to detect MreB filaments or polarized distribution of MreB monomers (Fig. 4*C*). MreB started to form small patches in Phase II. Compared to the WT spores where MreB patches mainly localized at nonpolar locations in germination Phase II, many MreB patches formed near cell poles and bulges of the emerging Δ*mglA* and Δ*mglB* cells (Fig. 4*C*), consistent with the altered distribution of RodA clusters. While MreB might localize at bulges in response to altered local cell curvatures in these mutants (33–38), the aggregation of MreB at their poles is likely due to the loss of the MglA-MglB polarity axis, because the poles of both WT and mutant cells have similar curvatures.

MglA connects MreB to the gliding motors, and the gliding motors drive the movement of MreB filaments (5, 7, 11). To test if MglA recruits the gliding motors to transport the Rod complexes to nonpolar locations through MreB, we investigated the regrowth process of the Δ*aglQS* pseudospores that are sonication-sensitive due to the lack of compact polysaccharide layers on their surfaces (39). Δ*aglQS* cells carry truncated gliding

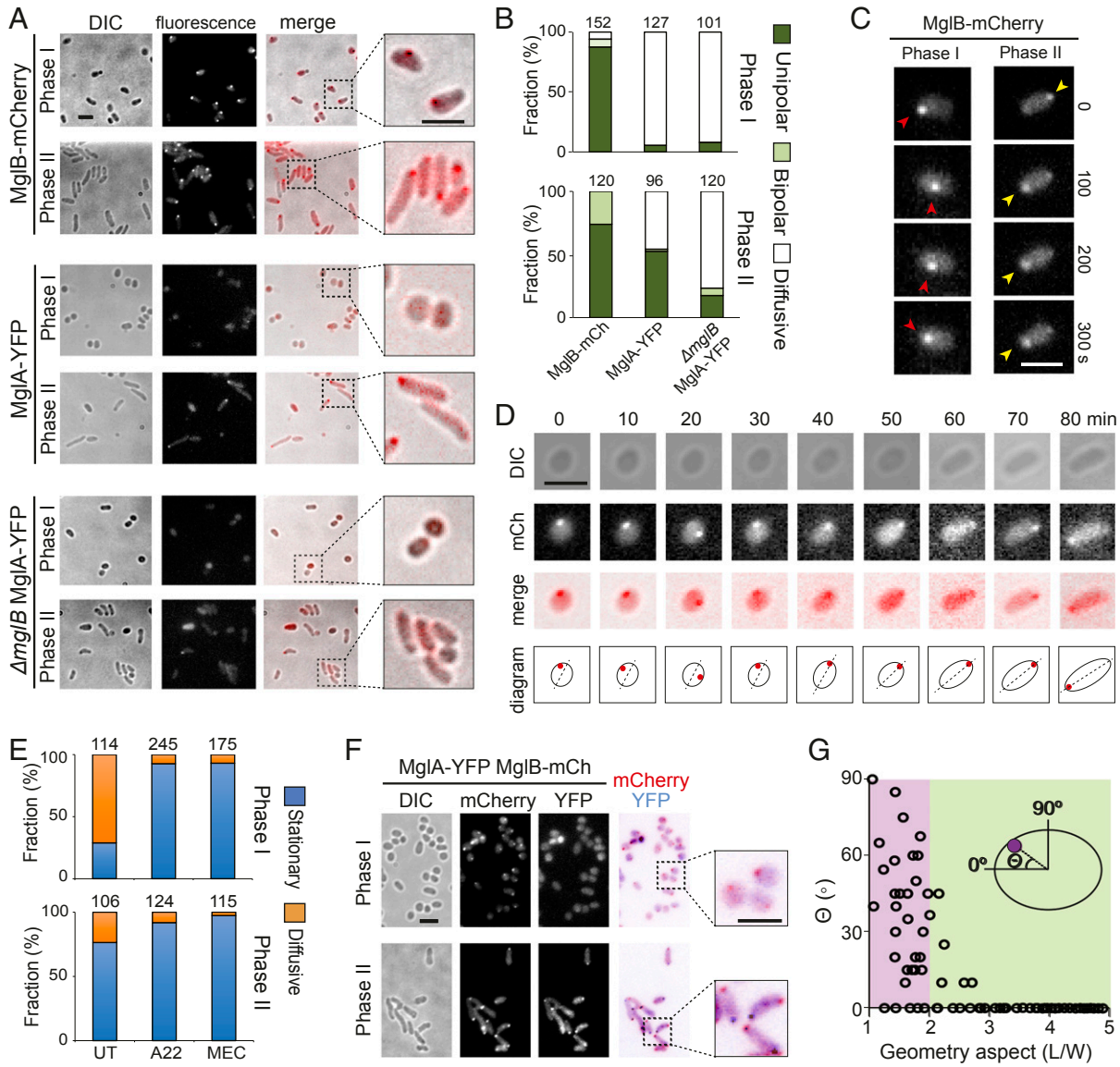

Fig. 3. MglB stabilizes at the first future pole. (*A*) While MglB-mCherry forms clusters in germination Phase I, MglA-YFP starts to form clusters in Phase II. In the absence of MglB, MglA-YFP forms significantly fewer clusters. (*B*) Quantification of the sequential stabilization of MglB and MglA clusters. The total number of spores/cells analyzed for each strain is shown on top of each bar. (*C*) The "wandering" dynamics of MglB clusters (red arrowhead) in Phase I spores (Movie S4). In Phase II, MglB clusters (yellow arrowhead) stabilized at cell poles and oscillated between opposite poles (Movie S6). (*D*) The localization of a MglB-mCherry cluster during the first 80 min of germination. As the MglB cluster stabilizes at one future pole, the emerging cell starts to elongate (Movie S5). The long axes of the spore/cell are marked with dashed lines. (*E*) Inhibitors of the Rod system, A22 and MEC, inhibit the wandering of MglB in both phases of germination. Images of emerging cells in Phase I and Phase II were captured at 1 h and 2 h of germination, respectively. For each treatment, the total number of MglB clusters analyzed is shown on top of each bar. UT, untreated. (*F*) MglA and MglB clusters stabilize at opposite cell poles in Phase II. (*G*) The stabilization of MglB clusters does not depend on local curvature. (Scale bars, 2 μm.)

motors that are unable to drive the rapid motion of MreB filaments (11). Phenocopying the Δ*mglA* and Δ*mglB* spores, elongation of Δ*aglQS* pseudospores delayed significantly (Fig. 2 *A* and *B*). Many emerging Δ*aglQS* cells displayed bulged surfaces in Phase II and survived at reduced rate, especially after hypoosmotic shock (Fig. 2 *A* and *E*). Consistently, significantly higher TADA staining was observed at cell poles and bulges in the elongation phase, similar to the observation made in Δ*mglA* Δ*dacB* and Δ*mglB* Δ*dacB* spores (Fig. 2*D*). Accordingly, significantly higher fractions of RodA clusters and MreB filaments were observed at poles and bulges in elongating Δ*aglQS* cells (Fig. 4 *B* and *C*). In summary, MglA and MglB restrict PG growth to nonpolar regions in germination Phase II utilizing the gliding motors, which transport MreB, and thus the whole Rod complexes, under the control of MglA.

Discussion

Phylogenetic studies revealed that rod-like shapes are ancestral to modern bacteria (40, 41). Establishing rod shape from primordial cells could have started with the development of PG cell wall (40, 42). As chemical-induced *M. xanthus* spores are PG-deficient, the sphere-to-rod transition during their germination provides a unique opportunity to study de novo PG synthesis and rod-like morphogenesis. Among all of the components tested in this study, only the Rod system is essential for the establishment of rod shape, in which MreB filaments provide spatial guidance for PG synthesis. We propose that in most rod-shaped bacteria

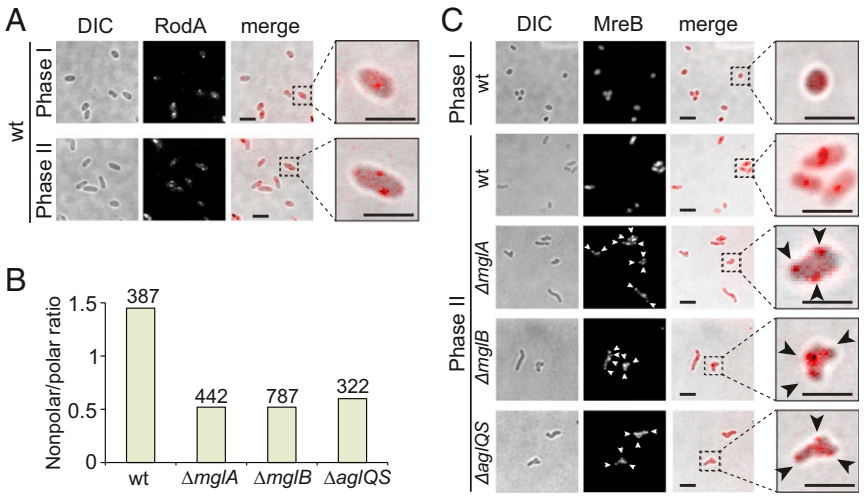

Fig. 4. The MglA-MglB polarity axis regulates the distribution of Rod complexes through MreB and the gliding motor. (*A*) RodA forms clusters in both phases of germination. (*B*) Nonpolar-to-polar distribution ratios of RodA clusters in the elongating cells of germination Phase II. The total number of RodA clusters analyzed is shown on top of each bar. (*C*) The localization patterns of MreB filaments. Consistent with the altered distribution of RodA cluster, MreB patches (arrowheads) are frequently detected near cell poles and bulges in the emerging Δ*mglA*, Δ*mglB*, and Δ*aglQS* cells in Phase II of germination. Images of emerging cells in Phase I and Phase II were captured at 1 h and 2 h of germination, respectively. (Scale bars, 2 μm.)

that contain MreB, expelling MreB from certain zones might be a common prerequisite for cell polarization and rod-like morphogenesis. Different organisms may achieve this goal using various mechanisms. First, in both *E. coli* and *B. subtilis*, the tendency of MreB filaments to localize at inwardly curved regions could be sufficient for the maintenance of rod shape (33, 34, 36, 38). Second, the composition of phospholipids in the cytoplasmic membrane could also provide localization cues for MreB. For instance, rafts of anionic phospholipids preferentially interact with MreB monomers and expel MreB filaments in *E. coli* (43). As a result, unaided by Mgl-like regulators and Agl-like motors, artificial spheres of *E. coli* and *B. subtilis* are able to regain rod shape. For example, PG-deficient L-forms of *E. coli* regain polarity and rod shape slowly, after several generations (44).

In *M. xanthus*, wandering MglB clusters survey the status of PG growth and the region where PG growth completes first in Phase I will host a MglB cluster and become a future pole in Phase II (Fig. 5). Once an MglB cluster stabilizes at one pole, the expulsion between MglB and MglA-GTP causes MglA-GTP to cluster at the opposite side of the spore. Because MglA-GTP connects to the Rod complexes through MreB filaments (4, 6, 7, 45), MglB clusters do not colocalize with the Rod complexes. Thus, MglB clusters respond to the status of PG synthesis indirectly through MglA. At the poles that contain MglB clusters, MglB expels MglA-GTP and, thus, the Rod complexes from the poles. At the opposite poles, MglA-GTP stimulates the assembly of the gliding machinery by directly connecting it to MreB (7, 14). Once assembled, the gliding machineries transport MreB filaments, which carry Rod complexes, away from the poles (5, 11) (Fig. 5). Taken together, the diametrically opposing clusters of MglA-GTP and MglB establish the polarity axis of the emerging cell, which restricts the activity of the Rod system to nonpolar locations through MreB.

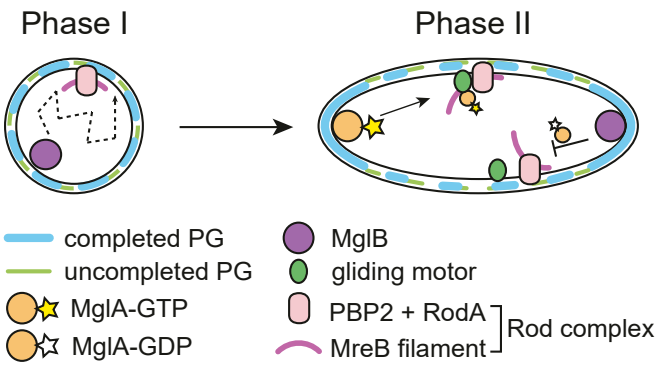

Fig. 5. A schematic model for the de novo establishment of rod shape by the MglA-MglB polarity axis.

Why are the Mgl and Agl components, nonessential for PG synthesis, important for spore germination? In contrast to fruiting bodies that require millions of cells and a few days to form, glycerol-induced sporulation mimics the natural process that individual *M. xanthus* cells form spores within hours in response to environmental stresses. Without the protection from the fruiting body, dispersed spores are vulnerable to biotic and abiotic environments during germination, before PG is fully synthesized (Fig. 2*E*). Thus, compared to other bacteria, the germination of chemical-induced *M. xanthus* spores faces additional challenges: (*i*) cell polarity has to be established de novo, (*ii*) PG has to be synthesized without template and (*iii*) both processes have to be completed rapidly. To cope with these challenges, *M. xanthus* utilizes the MglA-MglB axis to initiate polarization and recruits gliding motors to distribute MreB filaments rapidly to nonpolar regions (Fig. 5). This multimodule system provides great advantages for the survival of *M. xanthus* spores by facilitating rod-like morphogenesis within one generation. In contrast, neither the Mgl regulators nor the Agl gliding machineries are important for vegetative growth, where both PG and cell polarity already exist, as no growth or morphological defects were observed in vegetative *mgl* and *agl* cells.

Rather than dedicating to single functions, both the Agl and Mgl systems show remarkable versatility in *M. xanthus*. First, the Agl gliding motors are able to transport various cargos in different compartments of the cells: spore saccharides on cell surfaces (39), the Rod complex and some gliding proteins in the membrane and periplasm (12, 14), as well as MreB and other gliding proteins in the cytoplasm (11, 14, 46). Second, besides initiating polarization for rod-like morphogenesis, the Mgl system also controls two distinct motility systems in established rods. Localized to leading cell poles, the MglA GTPase interacts

with both Agl machineries and type IV pili (5, 7, 47), which not only produces gliding and twitching-like motility, respectively, but also provide a leading-lagging axis for cell movements.

GTPase-mediated cell polarization is not limited to *M. xanthus*. On the contrary, such mechanisms are rather universal in eukaryotes. Despite their enormous variety of polarized morphology, most eukaryotes control cell polarity through the Rho-family GTPase Cdc42 and its homologs, such as Rac in animals and Rop in plants (48). Cell polarization has been studied extensively in yeasts as yeast and human Cdc42 are about 80% identical (49). Similar to MglA-GTP, a single cluster of Cdc42-GTP determines cell polarity in the yeasts *Saccharomyces cerevisiae* and *Schizosaccharomyces pombe.* In both species, Cdc42 clusters are highly dynamic before stabilizing at the future polarity sites (49). *S. pombe* produces spherical spores that contain rigid outer cell walls (OCW). Cdc42, together with actin regulators and cell wall remodeling enzymes, assembles into a polar cap. As the spores of *S. pombe* germinate, the polar cap wanders during the isotropic growth phase before stabilizing at future poles to break symmetry through cytoskeletal elements and molecular motors (49, 50). Strikingly, similar to the connection between MglA and the Rod system, the association between Cdc42 and cell wall remodeling enzymes enables the polar cap to survey the status of OCW and to stabilize at the site of OCW rupture, which becomes the future pole of outgrowth (50). The similarities between the germination of *M. xanthus* and *S. pombe* spores suggest that the interplay between GTPase, cytoskeletons, cell wall-related enzymes, and molecular motors might be a conserved mechanism for cell polarization that has evolved before the divergence between prokaryotes and eukaryotes.

Materials and Methods

Sporulation, Spore Purification, and Germination. Vegetative *M. xanthus* cells were grown in liquid CYE medium (10 mM Mops pH 7.6, 1% [wt/vol] Bacto casitone [BD Biosciences], 0.5% yeast extract, and 4 mM $MgSO_4$) at 32 °C, in 125-mL flasks with rigorous shaking, or on CYE plates that contains 1.5% agar. When liquid cell culture reaches OD_{600} 0.1–0.2, glycerol was added to 1 M to induce sporulation. After rigorous shaking overnight at 32 °C, remaining vegetative cells were eliminated by sonication and sonication-resistant spores were purified by centrifugation (1 min, 15,000 × *g* and room temperature). The pellet was washed three times with water.

Microscopy Analysis. Cryo-ET was performed on a Polara G2 electron microscope. Images were collected at 9,000× magnification and 8-μm defocus, resulting in 0.42 nm per pixel. Data were acquired automatically with the SerialEM software (51). Time-lapse videos of the germination progress of WT and Δ*mglA* spores were recorded using an OMAX A3590U charge-coupled device (CCD) camera and a Plan Flour 40×/0.75 Ph2 DLL objective on a phase-contrast Nikon Eclipse 600 microscope. The length, width and geometric aspect ratios (L/W) of spores/cells were determined from differential interference contrast (DIC) images using a custom algorithm written in MATLAB (The MathWorks, Inc.), which is available upon request. DIC images of spores/cells were captured using a Hamamatsu ImagEM ×2 EM-CCD camera C9100-23B (effective pixel size 160 nm) on an inverted Nikon Eclipse-Ti microscope with a 100× 1.49 N.A. TIRF objective, which are also used for capturing fluorescence images. MglB and RodA clusters were localized using an algorithm written in MATLAB (11).

Data Availability. More detailed information is provided in *SI Appendix, Materials and Methods*. The codes used for cell dimension measurement and dynamic analysis of protein clusters are deposited in the GitHub repository, https://github.com/NanLabMyxo/Rod_shape_paper.

ACKNOWLEDGMENTS. We thank Autumn McManis and Elias Topo for technical assistance, Drs. Joseph Sorg and Ritu Shrestha for their help in the initial determination of germination phenotypes, Drs. Michael Van Nieuwenhze and Yen-Pang Hsu for providing TADA, and Drs. David Zusman, Michael Manson, and Joseph Sorg for critical reading of this manuscript. This work is supported by the National Institute of Health Grants R01GM129000 (to B.N.) and R01AI087946 (to J.L.) and by CNRS (to T.M.).

1. S. van Teeffelen, L. D. Renner, Recent advances in understanding how rod-like bacteria stably maintain their cell shapes. *F1000 Res.* **7**, 241 (2018).
2. H. Cho *et al*., Bacterial cell wall biogenesis is mediated by SEDS and PBP polymerase families functioning semi-autonomously. *Nat. Microbiol.* **1**, 16172 (2016).
3. T. K. Lee, K. Meng, H. Shi, K. C. Huang, Single-molecule imaging reveals modulation of cell wall synthesis dynamics in live bacterial cells. *Nat. Commun.* **7**, 13170 (2016).
4. S. Leonardy *et al*., Regulation of dynamic polarity switching in bacteria by a Ras-like G-protein and its cognate GAP. *EMBO J.* **29**, 2276–2289 (2010).
5. B. Nan *et al*., The polarity of myxobacterial gliding is regulated by direct interactions between the gliding motors and the Ras homolog MglA. *Proc. Natl. Acad. Sci. U.S.A.* **112**, E186–E193 (2015).
6. Y. Zhang, M. Franco, A. Ducret, T. Mignot, A bacterial Ras-like small GTP-binding protein and its cognate GAP establish a dynamic spatial polarity axis to control directed motility. *PLoS Biol.* **8**, e1000430 (2010).
7. A. Treuner-Lange *et al*., The small G-protein MglA connects to the MreB actin cytoskeleton at bacterial focal adhesions. *J. Cell Biol.* **210**, 243–256 (2015).
8. B. Nan, M. J. McBride, J. Chen, D. R. Zusman, G. Oster, Bacteria that glide with helical tracks. *Curr. Biol.* **24**, R169–R173 (2014).
9. E. M. Mauriello *et al*., Bacterial motility complexes require the actin-like protein, MreB and the Ras homologue, MglA. *EMBO J.* **29**, 315–326 (2010).
10. B. Nan, Bacterial gliding motility: Rolling out a consensus model. *Curr. Biol.* **27**, R154–R156 (2017).
11. G. Fu *et al*., MotAB-like machinery drives the movement of MreB filaments during bacterial gliding motility. *Proc. Natl. Acad. Sci. U.S.A.* **115**, 2484–2489 (2018).
12. B. Nan *et al*., Myxobacteria gliding motility requires cytoskeleton rotation powered by proton motive force. *Proc. Natl. Acad. Sci. U.S.A.* **108**, 2498–2503 (2011).
13. B. Nan *et al*., Flagella stator homologs function as motors for myxobacterial gliding motility by moving in helical trajectories. *Proc. Natl. Acad. Sci. U.S.A.* **110**, E1508–E1513 (2013).
14. L. M. Faure *et al*., The mechanism of force transmission at bacterial focal adhesion complexes. *Nature* **539**, 530–535 (2016).
15. D. R. Zusman, A. E. Scott, Z. Yang, J. R. Kirby, Chemosensory pathways, motility and development in *Myxococcus xanthus*. *Nat. Rev. Microbiol.* **5**, 862–872 (2007).
16. M. Dworkin, S. M. Gibson, A system for studying microbial morphogenesis: Rapid formation of microcysts in *Myxococcus xanthus*. *Science* **146**, 243–244 (1964).
17. E. I. Tocheva *et al*., Peptidoglycan transformations during *Bacillus subtilis* sporulation. *Mol. Microbiol.* **88**, 673–686 (2013).
18. K. Khanna *et al*., The molecular architecture of engulfment during *Bacillus subtilis* sporulation. *eLife* **8**, e45257 (2019).
19. N. K. Bui *et al*., The peptidoglycan sacculus of *Myxococcus xanthus* has unusual structural features and is degraded during glycerol-induced myxospore development. *J. Bacteriol.* **191**, 494–505 (2009).
20. K. A. O'Connor, D. R. Zusman, Starvation-independent sporulation in *Myxococcus xanthus* involves the pathway for beta-lactamase induction and provides a mechanism for competitive cell survival. *Mol. Microbiol.* **24**, 839–850 (1997).
21. T. K. Lee *et al*., A dynamically assembled cell wall synthesis machinery buffers cell growth. *Proc. Natl. Acad. Sci. U.S.A.* **111**, 4554–4559 (2014).
22. E. Kuru *et al*., In Situ probing of newly synthesized peptidoglycan in live bacteria with fluorescent D-amino acids. *Angew. Chem. Int. Ed. Engl.* **51**, 12519–12523 (2012).
23. E. Kuru, S. Tekkam, E. Hall, Y. V. Brun, M. S. Van Nieuwenhze, Synthesis of fluorescent D-amino acids and their use for probing peptidoglycan synthesis and bacterial growth in situ. *Nat. Protoc.* **10**, 33–52 (2015).
24. E. Kuru *et al*., Mechanisms of incorporation for D-amino acid probes that target peptidoglycan biosynthesis. *ACS Chem. Biol.* **14**, 2745–2756 (2019).
25. A. J. Meeske *et al*., SEDS proteins are a widespread family of bacterial cell wall polymerases. *Nature* **537**, 634–638 (2016).
26. Y. P. Hsu *et al*., Full color palette of fluorescent d-amino acids for *in situ* labeling of bacterial cell walls. *Chem. Sci.* **8**, 6313–6321 (2017).
27. M. F. Dion *et al*., *Bacillus subtilis* cell diameter is determined by the opposing actions of two distinct cell wall synthetic systems. *Nat. Microbiol.* **4**, 1294–1305 (2019).
28. A. Vigouroux *et al*., Class-A penicillin binding proteins do not contribute to cell shape but repair cell-wall defects. *eLife* **9**, e51998 (2020).
29. D. Keilberg, K. Wuichet, F. Drescher, L. Søgaard-Andersen, A response regulator interfaces between the Frz chemosensory system and the MglA/MglB GTPase/GAP module to regulate polarity in *Myxococcus xanthus*. *PLoS Genet.* **8**, e1002951 (2012).
30. C. B. Pogue, T. Zhou, B. Nan, PlpA, a PilZ-like protein, regulates directed motility of the bacterium Myxococcus xanthus. *Mol. Microbiol.* **107**, 214–228 (2018).
31. Y. Zhang, M. Guzzo, A. Ducret, Y. Z. Li, T. Mignot, A dynamic response regulator protein modulates G-protein-dependent polarity in the bacterium *Myxococcus xanthus*. *PLoS Genet.* **8**, e1002872 (2012).
32. T. Zhou, B. Nan, Exopolysaccharides promote *Myxococcus xanthus* social motility by inhibiting cellular reversals. *Mol. Microbiol.* **103**, 729–743 (2017).
33. B. P. Bratton, J. W. Shaevitz, Z. Gitai, R. M. Morgenstein, MreB polymers and curvature localization are enhanced by RodZ and predict *E. coli*'s cylindrical uniformity. *Nat. Commun.* **9**, 2797 (2018).
34. A. Colavin, H. Shi, K. C. Huang, RodZ modulates geometric localization of the bacterial actin MreB to regulate cell shape. *Nat. Commun.* **9**, 1280 (2018).
35. S. Hussain *et al*., MreB filaments align along greatest principal membrane curvature to orient cell wall synthesis. *eLife* **7**, e32471 (2018).

36. T. S. Ursell *et al*., Rod-like bacterial shape is maintained by feedback between cell curvature and cytoskeletal localization. *Proc. Natl. Acad. Sci. U.S.A.* **111**, E1025–E1034 (2014).
37. F. Wong, E. C. Garner, A. Amir, Mechanics and dynamics of translocating MreB filaments on curved membranes. *eLife* **8**, e40472 (2019).
38. R. M. Morgenstein *et al*., RodZ links MreB to cell wall synthesis to mediate MreB rotation and robust morphogenesis. *Proc. Natl. Acad. Sci. U.S.A.* **112**, 12510–12515 (2015).
39. M. Wartel *et al*., A versatile class of cell surface directional motors gives rise to gliding motility and sporulation in *Myxococcus xanthus*. *PLoS Biol.* **11**, e1001728 (2013).
40. P. R. J. Yulo, H. L. Hendrickson, The evolution of spherical cell shape; progress and perspective. *Biochem. Soc. Trans.* **47**, 1621–1634 (2019).
41. J. L. Siefert, G. E. Fox, Phylogenetic mapping of bacterial morphology. *Microbiology* **144**, 2803–2808 (1998).
42. J. Errington, K. Mickiewicz, Y. Kawai, L. J. Wu, L-form bacteria, chronic diseases and the origins of life. *Philos. Trans. R. Soc. Lond. B Biol. Sci.* **371**, 20150494 (2016).
43. T. Kawazura *et al*., Exclusion of assembled MreB by anionic phospholipids at cell poles confers cell polarity for bidirectional growth. *Mol. Microbiol.* **104**, 472–486 (2017).
44. G. Billings *et al*., *De novo* morphogenesis in L-forms via geometric control of cell growth. *Mol. Microbiol.* **93**, 883–896 (2014).
45. C. Galicia *et al*., MglA functions as a three-state GTPase to control movement reversals of *Myxococcus xanthus*. *Nat. Commun.* **10**, 5300 (2019).
46. M. Sun, M. Wartel, E. Cascales, J. W. Shaevitz, T. Mignot, Motor-driven intracellular transport powers bacterial gliding motility. *Proc. Natl. Acad. Sci. U.S.A.* **108**, 7559–7564 (2011).
47. I. Bulyha *et al*., Two small GTPases act in concert with the bactofilin cytoskeleton to regulate dynamic bacterial cell polarity. *Dev. Cell* **25**, 119–131 (2013).
48. C. F. Wu, D. J. Lew, Beyond symmetry-breaking: Competition and negative feedback in GTPase regulation. *Trends Cell Biol.* **23**, 476–483 (2013).
49. J. G. Chiou, M. K. Balasubramanian, D. J. Lew, Cell polarity in yeast. *Annu. Rev. Cell Dev. Biol.* **33**, 77–101 (2017).
50. D. Bonazzi *et al*., Symmetry breaking in spore germination relies on an interplay between polar cap stability and spore wall mechanics. *Dev. Cell* **28**, 534–546 (2014).
51. D. N. Mastronarde, Automated electron microscope tomography using robust prediction of specimen movements. *J. Struct. Biol.* **152**, 36–51 (2005).